Physica B 586 (2020) 412120

Contents lists available at ScienceDirect

Physica B: Physics of Condensed Matter

journal homepage: http://www.elsevier.com/locate/physb

Investigation of the local environment of SnO_2 in an applied magnetic field

J. Schell [a,b,*], T.T. Dang [b,c], D.V. Zyabkin [d,e], R.D. Mansano [f], D. Gaertner [g], A.W. Carbonari [h]

[a] European Organization for Nuclear Research (CERN), CH-1211, Geneva, Switzerland
[b] Institute for Materials Science and Center for Nanointegration Duisburg-Essen (CENIDE), University of Duisburg-Essen, 45141, Essen, Germany
[c] Helmholtz-Institut für Strahlen- und Kernphysik, University of Bonn, 53115, Bonn, Germany
[d] Chair Materials for Electrical Engineering and Electronics, Institute of Materials Science and Engineering, Institute of Micro and Nanotechnologies MacroNano®, TU Ilmenau, Gustav-Kirchhoff-Strasse 5, 98693, Ilmenau, Germany
[e] Department of Experimental Physics, Faculty of Science, Palacký University in Olomouc, 17. Listopadu 12, 77147, Olomouc, Czech Republic
[f] Escola Politécnica, Universidade de São Paulo, 05508-010, São Paulo, Brazil
[g] Institute of Materials Physics, University of Münster, D-48149, Münster, Germany
[h] Instituto de Pesquisas Energéticas e Nucleares, IPEN, São Paulo, SP, Brazil

ARTICLE INFO

Keywords:
Tin dioxide
Hyperfine interactions
Perturbed angular correlations
Magnetic field

ABSTRACT

This paper presents the results of time-differential perturbed gamma–gamma angular correlation measurements of SnO_2 thin films carried out in an applied magnetic field. The measurements were performed upon the implantation of Fe at 80 keV and ^{111}In (^{111}Cd) at 160 keV. The samples were further characterized by energy-dispersive X-ray spectroscopy. The hyperfine parameters were studied at room temperature with and without an applied magnetic field. The results indicate the presence of two distinct local environments for the probe nuclei. Both occupy a paramagnetic state and correspond to a substitutional Sn site in the rutile phase of SnO_2 with different numbers of electrons added to SnO_2:Cd^0. In addition, the crystal homogeneity of the site 1 increases upon applying the magnetic field.

1. Introduction

Tin dioxide (SnO_2) is a wide-bandgap n-type semiconductor that has excellent optical transparency and native oxygen vacancies; it also features a high carrier density and high thermal stability. SnO_2 is used in numerous applications including dye-sensitized solar cells and gas sensors [1–3]. Some time ago, it was shown that SnO_2 can exhibit room-temperature ferromagnetism depending on the doping and consequently on the inner structure [4–6]. However, despite numerous studies, no sound explanation for this phenomenon has been found. In fact, it was later acknowledged that transition-metal doping reduces the magnetic moment, and the increase in magnetic ordering is tied to both oxygen vacancies and the confinement of defects [7]. No ferromagnetism is detected in similar systems such as TiO_2, ZnO [8,9], and SnO_2 [10] in which hyperfine methods were used to implant a small quantity of probe material. Conversely, even with a negligible dopant concentration, online emission Mössbauer spectroscopy results in a plethora of defects due to online implantation measurements, making interpretation difficult. Thus, we present the results of time-differential perturbed gamma–gamma angular correlation (TDPAC) studies of SnO_2 in an applied magnetic field. This technique requires a smaller concentration of dopants and consequent annealing upon implantation may fully recover the structure.

The hyperfine properties of SnO_2 have been well studied, and various methods have been applied to probe the local environment. Generally, Sn conversion-electron Mössbauer spectroscopy applied to SnO_2 samples shows that Sn ions tend to occupy 2+ and 4+ states [11]. ^{57}Fe Mössbauer online studies show that SnO_2 features two charge states, Fe^{3+} and Fe^{2+}; the former exhibits spin-lattice relaxation, and the latter is attributed to recoil-caused interstitials [10]. TDPAC studies are the most profound and can include several isotopes of interest along with several types of samples, dopants, and annealing conditions. Upon implanting ^{111}In-(Cd) and annealing at 1023 K, Renteria et al. discovered that implantation at 400 keV resulted in two phases, SnO_2 [ω_Q = 18.4(1), η = 0.18(2)] and SnO, which were later transformed into a single phase of SnO_2 [11]. Although the hyperfine parameters coincided with previous reports [12,13], there was no dynamic interaction.

Ramos et al. studied hyperfine interactions by implanting ^{111}In-(Cd) into SnO_2 thin films at 160 keV and investigating the system over a broad temperature range (up to 923 K). The results revealed two

* Corresponding author. European Organization for Nuclear Research (CERN), CH-1211, Geneva, Switzerland.
E-mail address: juliana.schell@cern.ch (J. Schell).

https://doi.org/10.1016/j.physb.2020.412120
Received 13 December 2019; Received in revised form 28 January 2020; Accepted 20 February 2020
Available online 4 March 2020

fractions; the substitutional site was characterized by ω_Q ~16.7 Mrad/s and η ~0.1 [14]. Recently, Darriba et al. [15] reported the combined dynamic and static quadrupole interactions (the so-called on–off model) complemented by ab initio calculations. The combined interactions were induced by an increase in the hole concentration as the temperature decreased, which was attributed to a shortage of electrons caused by the reduced thermal ionization of defects. The ω_Q and η values for the local environment 1 were ~17 Mrad/s and ~0.2, respectively, while those of second fraction were ~22.5 Mrad/s and ~0.5, respectively [15]. Only above 650 K and 923 K, respectively, these interactions become purely static. Table 1 lists most of the parameters from previous works involving TDPAC with In as a probe isotope.

Applying a magnetic field can be advantageous because it increases sample homogeneity during sample preparation. For instance, during the fabrication of homogenized SnO_2 nanowires, a temperature gradient was found to be very important, especially under an applied magnetic field [17]. Moreover, such magnetically enhanced nanowires are more responsive to gaseous sulfur compounds [17]. The study of local phenomenology is useful to better understand the atomistic effects of external magnetic fields. Therefore, in this study, we used TDPAC to investigate the local effects of an applied magnetic field on SnO_2 samples.

2. Time-differential perturbed gamma–gamma angular correlation method

Due to the suitable nuclear properties (i.e., spin 5/2) and relatively long half-life of the parent ^{111}In nuclei, the evolution of the local environment can be followed with high sensitivity by measuring the perturbation function $R(t) \approx A_{22}G_{22}(t)$, where

$$G_{22}(t) = s_0 + \sum_{n=1}^{3} s_n(\eta)cos[\omega_n(\eta)t] \quad (1)$$

is the perturbation factor, with ω_n being the transition frequencies between two M states. The mentioned perturbation factor is valid for nuclear spin $I = 5/2$ of the intermediate state of the daughter ^{111}Cd probe nuclei. Moreover, if probe atoms are exposed to j different lattice environments (sites), and each of them creates a characteristic field gradient at a fraction f of the probe-atom sites, the perturbation function becomes $R(t) = A_{22}\sum_j f_j G_{22}^j(t)$. The observable ω_n frequencies are given by $\omega_n = 6\omega_Q C_n(\eta)$. The coefficient C_n can be numerically calculated for a known η [18]. Additionally, the coefficients s_n denote the amplitudes of the transition frequencies ω_n and are summations of the Wigner 3j symbol products that run over the allowed magnetic-field-split hyperfine states. Besides, the axial asymmetry of the electric field gradient tensor or deviations from it are described using the asymmetry parameter $\eta = (V_{xx} - V_{yy})/V_{zz}$. The primary component V_{ZZ} of the electric field gradient tensor can be obtained from the nuclear quadrupole frequency ω_Q as follows:

$$\omega_Q = \frac{eQV_{zz}}{4I(2I-1)\hbar}, \quad (2)$$

where Q is the nuclear quadrupole moment. Furthermore, the lowest transition frequency ω_0 is the hyperfine parameter considered in this work and describes the experimental nuclear quadrupole interactions. Additional details about the TDPAC technique can be found in Refs. [19, 20].

In the presence of a magnetic field, the TDPAC technique is also suitable for measuring magnetic contributions to the hyperfine fields, and the perturbation function is given by [21].

$$R(t) = A_{22}\left\{f\left[s_0 + s_1 cos(\omega_L t)exp\left(\frac{-(\Delta\omega_L t)^2}{2}\right) + s_2 cos(2\omega_L t)exp\left(\frac{-(2\Delta\omega_L t)^2}{2}\right)\right] + (1-f)\right\} \quad (3)$$

Pure-magnetic-dipole interactions have frequencies $\omega_1 = \omega_L$ and $\omega_2 = 2\omega_L$, where $\omega_L = \left(\frac{\mu}{I}\right)B_{HF}$ is the Larmor frequency. Here, $\mu = 0.7656\mu_N$, where μ_N is the nuclear magneton, and $I = \frac{5}{2}\hbar$. The coefficient f is the amplitude of the modulation, which is related to the fraction of TDPAC probes occupying an environment that produces a nonzero B_{HF}, and A_{22} is the anisotropy coefficient of the γ–γ cascade. The argument of the exponential term contains $\Delta\omega_L$, which reflects a distribution about the modulation frequencies caused by slight perturbations of the probe atom. For the experiments in this study, we assume a Lorentzian frequency distribution.

In the presence of both magnetic and electric hyperfine interactions, the analysis of the combined interaction in the TDPAC spectra is very complex. Its formalism is given by [22,23].

$$G_{k_1k_2}^N = \frac{1}{2}\sum_n a_{nN}^{k_1k_2}\left[\frac{1}{1+(n\omega_Q\tau + N\omega_L\tau)^2}H(n\omega_Q\tau + N\omega_L\tau) + \frac{+1}{1+(n\omega_Q\tau - N\omega_L\tau)^2}H(n\omega_Q\tau - N\omega_L\tau)\right], \quad (4)$$

where $a_{nN}^{k_1k_2}$ is a weighting factor, and τ is the lifetime of the intermediate state ($\tau = 84.5$ ns for $I = 5/2$). In particular, the perturbation function (4) cannot be solved analytically and must be computed numerically. Furthermore, the angular correlation function depends strongly on η, β (the orientation of the magnetic field direction with V_{zz}), $y = \frac{\omega_L}{\omega_Q}$ (the ratio of the Larmor frequency to the quadrupole interaction), and α (a second Euler angle), as shown by Alder et al. [22]. In this study, the TDPAC technique was used to measure the hyperfine parameters in SnO_2 thin films with and without an applied magnetic field.

Table 1
Hyperfine interaction parameters obtained at room temperature for the ^{111}In (^{111}Cd) isotope and for different types of samples along with different methods to introduce ^{111}In into the samples.

ω_Q Mrad/s	η	Type of sample	Method of probe incorporation	Reference
22.5	0.5	Powder	Diffused In	[15]
17	0.2			
18.2 (1)	0.1(1)	Powder	Diffused In	[13]
31.1 (9)	0.45 (4)	Oxidized Sn foils, powders	Diffused In	[12]
14.3 (6)	0.65			
28.8 (1)	0.52 (5)	Thin films	Diffused In	[16]
14.9 (6)	0.58 (6)			
18.4 (1)	0.18 (2)	Thin films	Implanted In	[11]
16.7	0.1	Thin films	Implanted In	[14]

3. Experiment

Thin films with thicknesses of ~100 nm were deposited on Si(100) substrates by magnetic sputtering. The ^{111}In probe nuclei were ion-implanted with an energy of 160 keV after the implantation of 1% Fe at 80 keV. The implantations were performed at the Bonn Isotope Separator (BONIS) ion implanter [24,25], as described in Ref. [26]. Ion implantation was followed by heating to 873 K in air for 10 min. Approximate full-cascade SRIM calculations [27] indicated an ion range of ~40 nm (38 and 42 nm for Fe and In ions, respectively) and approximately 18 nm of straggle (see Fig. 1a). Fig. 1b presents SRIM calculations [27] of the Sn vacancies (V_{Sn}) and O vacancies (V_O) created by the implantation of ^{111}In and Fe ions.

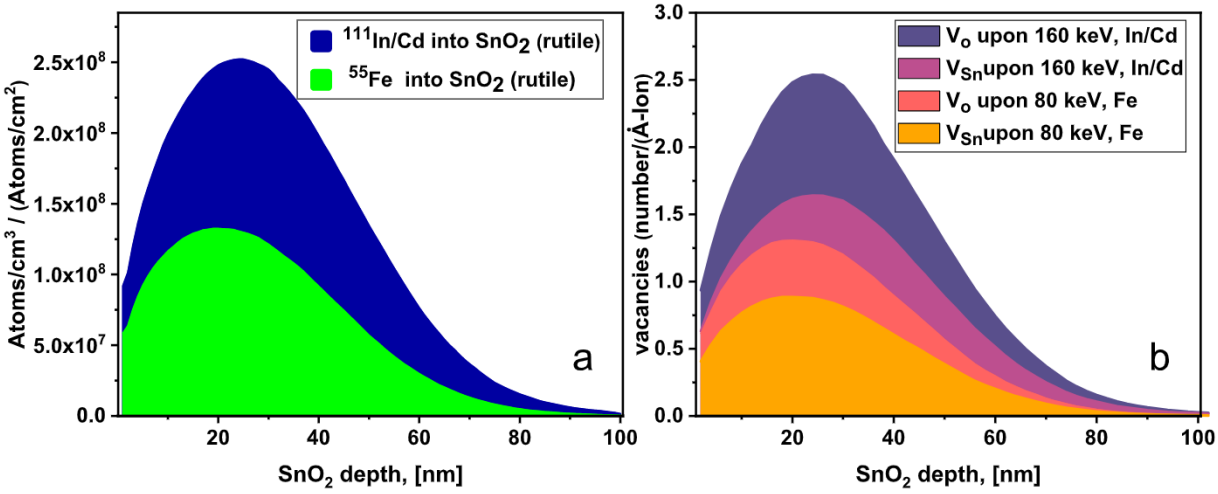

Fig. 1. (a) Full-cascade SRIM implantation profiles for Fe and In/Cd. (b) Sn and O vacancies profile estimation for the In and Fe implantations.

The hyperfine parameters were measured at room temperature (RT). The measurements were taken with and without an applied magnetic field of 2.1 T [28]. Fig. 2 shows a schematic diagram of the magnet apparatus, which had a radius of 5 cm and lead housing. The two permanent magnets were separated by 2.4 mm and produced in this space a 2.1-T magnetic field. To reduce gamma-ray absorption and scattering, the cylindrical pot had 12 radial windows. The samples were positioned inside the pot facing down toward the detector plane.

Energy-dispersive X-ray spectroscopy (EDS) was performed on the SnO_2 thin films after the TDPAC experiments. The EDS measurements were conducted at 20 kV.

4. Results and discussion

Fig. 3 shows the RT perturbed angular correlation spectra of the thin films after maintaining the films in air at 873 K for 10 min (thermal treatment in air). The upper spectrum belongs to a sample with no field, while the bottom spectrum was obtained from a sample in an applied magnetic field of 2.1 T. The blue lines are fits that give the hyperfine parameters, which are presented in Table 2.

Observable changes in spectra measured with the sample in an applied magnetic field of 2.1 T are mainly due to the applied magnetic field, which gives rise to a Larmor frequency of $\omega_L = 32$ Mrad/s. However, the hyperfine parameters show no evidence of magnetic interactions for the pure sample beyond those from the 2.1-T magnetic field.

The results show that the magnetic field affects site 1 more than site 2. Comparison with previous studies [14,29,30] carried out after thermal treatment in vacuum or under a nitrogen atmosphere shows that using ^{111}In as probe nuclei when annealing at 873 K in air is not sufficient to remove all defects caused by the implantation process. This means that a considerable amount of oxygen vacancies were created;

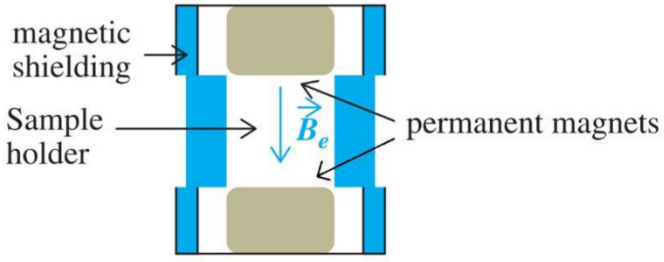

Fig. 2. Schematic diagram of the magnetic field setup used in this work.

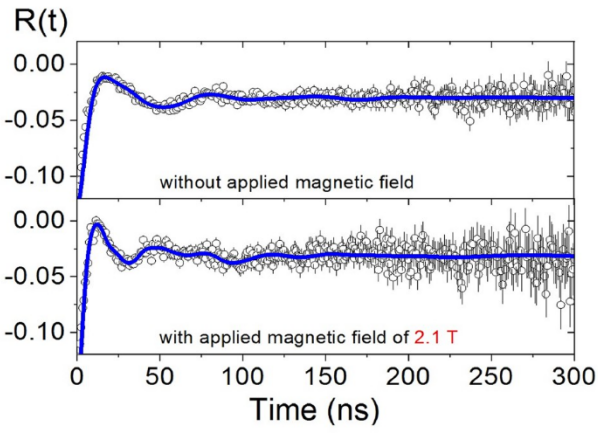

Fig. 3. TDPAC spectra of thin films measured at RT without (top) and with (bottom) an applied magnetic field of 2.1 T. The blue solid curves show the least-squares fits that give the hyperfine parameters. (For interpretation of the references to colour in this figure legend, the reader is referred to the Web version of this article.)

therefore, we cannot disregard the influence of these vacancies on paramagnetism, which arises from interactions between the defects and the applied magnetic field. Moreover, the oxygen vacancies lead to high charge–hole mobility, which is important for applications. Since the presence of the $^{111}In^{3+}$ probe results in a charge imbalance, it is possible that oxygen vacancies and In are near-neighbors [12].

Due to the type of magnet-pot housing used in these experiments and its size, samples with relatively high activity were required to obtain sufficient statistics. Note that increasing the implantation dose creates more defects; the process can damage the upper layers down to 40 nm and produce interstitials and vacancies. Additionally, the metal present in the housing causes significant gamma-ray scattering, which reduces the gamma anisotropy.

The TDPAC results indicate the presence of two sites for the probe nuclei. The substitutional Sn site in the well-known rutile phase of SnO_2 presents two different local environments, referred to as site 1 and site 2. Upon applying a magnetic field, paramagnetic hyperfine interactions were detected at both sites.

The dominant local environment, site 2, has an electric field gradient of 5.75×10^{21} V/m^2 for $Q = 0.641(25)$ [31] or 4.82×10^{21} V/m^2 for $Q = 0.765(15)$ [32] and an asymmetry parameter of 0.37(1). Considering $Q = 0.765(15)$, our values are consistent with the theoretical electric field gradient and asymmetry parameter of 5.11×10^{21} V/m^2 and 0.36,

Table 2
Hyperfine parameters obtained from measurements made using ^{111}In as probe nuclei. The frequencies ω_Q and ω_L are given in Mrad/s.

	f_1 (%)	ω_{Q1}	ω_{L1}	η_1	δ_1 (%)	f_2 (%)	ω_{Q2}	ω_{L2}	η_2	δ_2 (%)
0 T	32(5)	19(1)	–	0.32(3)	19(2)	68(10)	14(1)	–	0.37(1)	20(1)
2.1 T	46(5)	17(1)	32(1)	0.17(3)	12(1)	54(6)	26(3)	25(2)	0.45(2)	15(2)
	site 1					site 2				

respectively, obtained by Darriba et al. [15] from powder samples in a neutral cell (SnO_2:Cd^0) using the Perdew-Burke-Ernzerhof generalized gradient approximation (PBE-GGA). This local environment can be assigned to the metastable state of Cd^0 at a substitutional Sn site in SnO_2. The SnO_2:Cd^0 notation is used when a (neutral) Cd atom replaces a (neutral) Sn one in SnO_2 oxide, i. e., none electron is added to the system to compensate the smaller valence of impurity (Cd^{2+}) atom when substituting the host atom (Sn^{4+}). The value we chose for the nuclear quadrupole moment of the 245-keV $5/2^+$ level of the ^{111}Cd probe, Q = 0.765(15) b [32], is close to that reported by Errico et al. [33], Q = 0.76 (2) b.

Moreover, with a nonzero applied magnetic field, the nuclear quadrupole interaction frequency of site 2 increases strongly from 14(1) to 26(3) Mrad/s. This value is similar to that obtained for thin films at room temperature [28.8(1) Mrad/s] [16]. The magnetic field affects the metastable state of Cd^0. Considering Q = 0.765(15) b, our electric field of 9×10^{21} V/m^2 is too strong and cannot be compared to any simulated values from the work of Darriba et al. [15].

Conversely, with no applied magnetic field, the electric field gradient at the site 1 is 6.5×10^{21} V/m^2 for Q = 0.765(15) b [32], and the asymmetry parameter is 0.32(3). These results are comparable to simulation results based on the local density approximation for a charged impurity state with 1.8–2.0 electrons added to SnO_2:Cd^0 [15]. By applying a magnetic field, the electric field gradient for Q = 0.765 (15) b [32] is 5.85×10^{21} V/m^2. These results are consistent with the PBE-GGA result of 5.75×10^{21} V/m^2 with an asymmetry parameter of 0.19 [15] for SnO_2:Cd^{2-} with two electrons added to the system. We therefore associate this local environment with Cd at substitutional Sn sites with 1.8–2.0 electrons added to SnO_2:Cd^0. The curious point is that the applied magnetic field has somehow increased the number of electrons in the local environment.

Interestingly, the results indicate that upon applying the magnetic field, the width of the nuclear quadrupole interaction frequency decreases at both sites. This frequency distribution is a crucial parameter for measuring the homogeneity of the crystal; thus, this result indicates that the local environment is more homogeneous in an applied magnetic field than in its absence. A similar effect was detected in AlN using the TDPAC technique [34]. Note that a magnetic field affects structural defects even in their pre-existing metastable states [35].

Crystal lattice imperfections mainly affect the electric field gradient tensor [36] by distributing its tensor components around the values of a perfect crystal lattice [36]. The asymmetry parameter of site 1 decreases significantly from 0.32(3) to 0.17(3) upon applying a magnetic field, which is a second indication that the applied magnetic field improves the crystal homogeneity. However, the increase in the asymmetry parameter of site 2 from 0.37(1) to 0.45(2) cannot be easily explained. This increase means that the local point symmetry of this particular site is disturbed by the applied magnetic field. If this site is associated with oxygen vacancies, it may be possible that the interaction between the applied magnetic field and the vacancies promotes an imbalance near the probe nuclei, thereby increasing the asymmetry [37].

The application of an external magnetic field reveals the paramagnetic nature of SnO_2, which is consistent with the results of all previous TDPAC experiments, including recent results obtained for thin films using ^{117}In and ^{111}Cd as probe nuclei [38]. Garcia et al. [39] argued that the observed ferromagnetism, which has quite frequently been reported in the literature, is due to sources other than intrinsic ferromagnetism. Ferromagnetism in semiconductor oxides remains debatable because the essential issues of uniformity and reproducibility have yet to be unraveled [40].

Fig. 4 presents the EDS spectrum, which show the signals of tin, iron, and oxygen from the sample, a pronounced peak of silicon from the substrate, and a signal corresponding to a small concentration of Cu impurity, which was contributed by the target holder during thin film deposition. The samples were coated with platinum before EDS analysis to improve conductivity. The target holder used during sputtering was composed of cupper; however, an electrostatic shield in the target was used to reduce the plasma and consequent sputtering of the target. Nevertheless, Cu contamination occurs under certain process conditions, as confirmed by EDS analysis in this study. We understand that Cu contamination, even at very low quantities, may affect the hyperfine parameters. Therefore, new experiments without Cu contamination will be performed for comparison with the results of this work. Moreover, additional experiments with ^{111m}Cd are required to better understand how electron capture nuclear transmutation affects the ^{111}In probe in the samples, and if this effect can be observed under an applied external magnetic field. In this case, the measurements are subject to the electron conversion process of the ^{111m}Cd probe. The influence of Fe and Cu in possible charge recombination process can be further investigated by comparing the results obtained with ^{111m}Cd and ^{111}In probes. Future research along these lines was proposed at ISOLDE-CERN [41] within the solid-state physics program [42,43] as experiment LOI144 [44]. After these investigations, we intend to simultaneously implant ^{111}In and ^{111m}Cd [45] for comparison.

The abovementioned TDPAC experiments should be complemented with self-diffusion experiments [46]. The diffusion of Cd into SnO_2 thin films strongly depends on the conditions of the heat treatment. Napo et al. deposited SnO_2 thin films with a thin Cd layer and annealed them

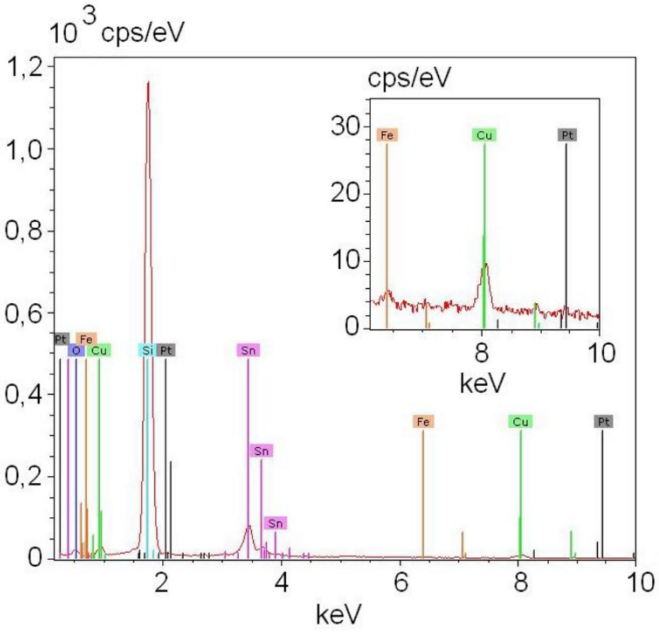

Fig. 4. EDS spectrum of SnO_2 thin film measured after the TDPAC experiments. The inset shows a zoomed-in view of the interval from 6.5 to 10 keV for a better view of the Cu peak.

at 850 K for 30 min under argon flow [47]. Depth profiles obtained using X-ray photoelectron spectroscopy show that Cd diffuses along the grain boundaries. Due to the improvement of the grain boundary quality, the conductivity could be increased by approximately a factor of two. After annealing at the same temperature for the same duration but under air instead of Ar, CdO was formed at the surface, prohibiting the diffusion of Cd into the SnO_2 layer.

In-diffusion was investigated by Ray et al. to obtain SnO_2/ITO bilayer films with good electrical and optical properties for the transparent electrodes of amorphous silicon solar cells [48]. In this work, the diffusion of indium through the SnO_2 layer into the p and i layers was observed by secondary-ion mass spectroscopy. The thickness of the SnO_2 layer was increased, allowing the deposition of the p layer at temperatures up to 180 °C without enhancing indium diffusion. To our knowledge, no previous studies have investigated Fe diffusion in SnO_2.

In undoped SnO_2 the electrical conductivity depends on electrons resulting of a stoichiometry deviation in the material composition. As mentioned above, under atomistical view, these deviations are caused by lattice defects (vacancies or interstitials) [49,50]. Here, the vacancies correspond to oxygen and the interstitials to tin. In single-crystalline material, a resistivity dependency of 1/6 power was observed for double ionized oxygen vacancies [50]. Advani et al. investigated the diffusion kinetics of the oxygen vacancies by introducing a controlled amount of oxygen in SnO_2 thin-films annealed under a high-vacuum at 200 °C for 360 h [51]. During the heat treatment under vacuum, a large amount of oxygen vacancies are incorporated in relaxing to the equilibrium conductivity value. Introducing subsequently oxygen into the thin-film a net-motion of the vacancies from the bulk to the surface was caused (diffusion of Oxygen into the bulk). Therefore, the resistance increased following a squareroot of time behaviour and a diffusion coefficient of $D_O = 1.4 \times 10^{-17}$ m^2s^{-1} was obtained [51].

5. Conclusions

Measurements of SnO_2 thin films in an applied magnetic field suggest the presence of two different local environments with distinct paramagnetic hyperfine interactions at room temperature. The effect of the applied magnetic field on the film reveals the paramagnetic nature of SnO_2 thin film and increases crystal homogeinity of site 1. Implantation-induced defects cause small changes in the hyperfine parameters of the second site, which has a slightly lower Larmor frequency. Both local environments can be associated with Cd at substitutional Sn sites with 1.8–2.0 electrons added to SnO_2:Cd^0. In future work, we intend to measure the samples after different thermal treatments to better understand how an applied magnetic field affects the crystal lattice defects. Measurements using ^{111m}Cd as a probe are also foreseen.

Author contributions

J. Schell wrote the manuscript with contributions from T. T. Dang, D. V. Zyabkin and D. Gaertner. R. Mansano was responsible for sample preparation. A. W. Carbonari supervised the work and contributed to the writing of the manuscript.

Declaration of competing interest

The authors declare no conflict of interest.

Acknowledgments

This research was funded by the Federal Ministry of Education and Research (BMBF) through Grant Nos. 05K16PGA and 05K16SI1, 05K19SI1 “eMMA” and from the DAAD/CNPq through Grant No. 290102/2011-1. We thank PD R. Vianden, Ms. C. Noll, and the BONIS team at HISKP, Bonn, for the implantations and their warm hospitality.

References

[1] W. Göpel, K.D. Schierbaum, Sensor. Actuator. B Chem. 26 (1995) 1.
[2] A.N.M. Green, E. Palomares, S.A. Haque, J.M. Kroon, J.R. Durrant, J. Phys. Chem. B 109 (2005) 12525.
[3] P.W. Park, H.H. Kung, D.W. Kim, M.C. Kung, J. Catal. 184 (1999) 440.
[4] T. Dietl, H. Ohno, F. Matsukura, J. Cibert, D. Ferrand, Science 287 (2000) 1019.
[5] K.C. Verma, R.K. Kotnala, Phys. Chem. Chem. Phys. 18 (2016) 17565.
[6] J. Zhang, R. Skomski, L.P. Yue, Y.F. Lu, D.J. Sellmyer, J. Phys. Condens. Matter 19 (2007) 256204.
[7] N.H. Hong, N. Poirot, J. Sakai, Phys. Rev. B 77 (2008), 033205.
[8] H.P. Gunnlaugsson, R. Mantovan, H. Masenda, T.E. Mølholt, K. Johnston, K. Bharuth-Ram, H. Gislason, G. Langouche, D. Naidoo, S. Ólafsson, A. Svane, G. Weyer, J. Phys. Appl. Phys. 47 (2014), 065501.
[9] R. Mantovan, H.P. Gunnlaugsson, K. Johnston, H. Masenda, T.E. Mølholt, D. Naidoo, M. Ncube, S. Shayestehaminzadeh, K. Bharuth-Ram, M. Fanciulli, H. P. Gislason, G. Langouche, S. Ólafsson, L.M.C. Pereira, U. Wahl, P. Torelli, G. Weyer, Adv. Electron. Mater. 1 (2015) 1400039.
[10] H.P. Gunnlaugsson, K. Nomura, T.E. Mølholt, S. Shayestehaminzadeh, K. Johnston, R. Mantovan, H. Masenda, M. Ncube, K. Bharuth-Ram, H. Gislason, G. Langouche, D. Naidoo, S. Ólafsson, G. Weyer, I.C. the, Hyperfine Interact. 226 (2014) 389.
[11] M. Renteria, A.G. Bibiloni, M.S. Moreno, J. Desimoni, R.C. Mercader, A. Bartos, M. Uhrmacher, K.P. Lieb, J. Phys. Condens. Matter 3 (1991) 3625.
[12] A.G. Bibiloni, J. Desimoni, C.P. Massolo, M. Rentería, Phys. Rev. B 38 (1988) 20.
[13] H. Wolf, S. Deubler, D. Forkel-Wirth, H. Foettinger, M. Iwatschenko-Borho, F. Meyer, M. Renn, W. Witthuhn, R. Helbig, Mater. Sci. Forum 10–12 (1986) 863.
[14] J.M. Ramos, T. Martucci, A.W. Carbonari, M. de Souza Costa, R.N. Saxena, R. Vianden, Hyperfine Interact. 221 (2013) 129.
[15] G.N. Darriba, E.L. Muñoz, A.W. Carbonari, M. Rentería, J. Phys. Chem. C 122 (2018) 17423.
[16] M.S. Moreno, A.G. Bibiloni, C.P. Massolo, J. Desimoni, M. Rentera, Phys. Rev. B 40 (4) (1989) 2546–2548.
[17] J.C. Briones, G. Castillon, M.P. Delmo, G.N.C. Santos, J. Nanomater. 2017 (2017) 4396723.
[18] M. Forker, Nucl. Instrum. Methods l06 (1973) 121.
[19] A. Abragam, R.V. Pound, Phys. Rev. 92 (1953) 943.
[20] H. Frauenfelder, R.M. Steffen, K. Siegbahn, in: K. Siegbahn (Ed.), α-, β- and γ-Ray Spectroscopy, North-Holland, 1965.
[21] H. Wolf, Z. Guan, S. Lauer, H. Natter, M. Schmelzer, R. Hempelmann, T. Wichert, J. Metastable Nanocryst. Mater. 8 (2000) 847.
[22] K. Alder, E. Matthias, W. Schneider, R.M. Steffen, Phys. Rev. 129 (1963) 1199.
[23] E. Matthias, W. Schneider, R.M. Steffen, Phys. Rev. 125 (2012) 261.
[24] K. Freitag, Radiat. Eff. 44 (1979) 185.
[25] Group Vianden, Time-differential perturbed angular correlations, Helmholtz-Institut für Strahlen- und Kernphysik (HISKP). http://tdpac.hiskp.uni-bonn.de/pac/. (Accessed July 2017).
[26] J. Schell, D.C. Lupascu, A.W. Carbonari, R.D. Mansano, I.S. Ribeiro Jr., T.T. Dang, I. Anusca, H. Trivedi, K. Johnston, R. Vianden, J. Appl. Phys. 121 (2017) 145302.
[27] J.F. Ziegler, M. Ziegler, J. Biersack, Nucl. Instrum. Methods Phys. Res. B 268 (2010) 1818.
[28] I. Alfter, E. Bodenstedt, B. Hamer, W. Knichel, R. Müßeler, R. Sajok, T. Schaefer, J. Schüth, R. Vianden, Zeitschrift für Physik A Hadrons and Nuclei, vol. 347, 1993, p. 1.
[29] J.M. Ramos, A.W. Carbonari, T. Martucci, M.S. Costa, G.A. Cabrera-Pasca, M.A. V. Macedo, R.N. Saxena, Phys. Procedia 28 (2012) 90–94.
[30] J.M. Ramos, A.W. Carbonari, M.S. Costa, R.N. Saxena, Hyperfine Interact. 197 (1) (2010) 239–243.
[31] H. Haas, A.P. Stephan, L.B.S. Hemmingsen, V. Kellö, P.W. Zhao, Europhys. Lett. 117 (2017) 62001.
[32] H. Haas, J.G. Correia, Hyperfine Interact. 198 (2010) 133.
[33] L. Errico, K. Lejaeghere, J. Runco, S.N. Mishra, M. Rentería, S. Cottenier, J. Phys. Chem. C 120 (2016) 23111.
[34] I. Agarwal, P. Kessler, R. Vianden, Hyper. Interact. 221 (2013) 117.
[35] Y.I. Golovin, R.B. Morgunov, J. Exp. Theor. Phys. 88 (1999) 332.
[36] M. Forker, Nucl. Instrum. Methods 106 (1973) 121.
[37] F.H. Aragón, L. Villegas-Lelovsky, J.B.L. Martins, J.A.H. Coaquira, R. Cohen, L.C.C. M. Nagamine, P.C. Morais, J. Phys. Appl. Phys. 50 (2017) 115103.
[38] J. Schell, D.C. Lupascu, A.W. Carbonari, R.D. Mansano, R.S. Freitas, J. N. Goncalves, T. Thanh Dang, R. Vianden, ISOLDE Collaboration, J. Appl. Phys. 121 (2017) 195303.
[39] M.A. Garcia, E. Fernandez Pinel, J. de la Venta, A. Quesada, V. Bouzas, J. F. Fernández, J.J. Romero, M.S. Martín González, J.L. Costa-Krämer, J. Appl. Phys. 105 (2009), 013925.
[40] L.M.C. Pereira, J.P. Araujo, M.J. Van Bael, K. Temst, A. Vantomme, J. Phys. Appl. Phys. 44 (2011) 215001.
[41] R. Catherall, W. Andreazza, M. Breitenfeldt, A. Dorsival, G.J. Focker, T.P. Gharsa, T. Giles, J.-L. Grenard, F. Locci, P. Martins, S. Marzari, J. Schipper, A. Shornikov, T. Stora, J. Phys. G Nucl. Part. Phys. 44 (2017), 094002.
[42] K. Johnston, J. Schell, J.G. Correia, M. Deicher, H.P. Gunnlaugsson, A.S. Fenta, E. David-Bosne, A.R.G. Costa, D.C. Lupascu, J. Phys. G Nucl. Part. Phys. 44 (2017) 104001.
[43] J. Schell, P. Schaaf, D.C. Lupascu, Perturbed angular correlations at ISOLDE: a 40 years young technique, AIP Adv. 7 (2017) 105017.
[44] A.W. Carbonari, R.N. Saxena, J. Mestnik-Filho, A.L. Lapolli, C.O. Sena, G.A. C. Pasca, F.H.M. Cavalcante, L.F.D. Pereira, J.M. Ramos, E. Muñoz, A.M. Lopes, J. G. Correia, Local investigation with radioactive probe of wide band gap oxides thin

films doped with transition metals, Letter of Intent to the ISOLDE and Neutron Time-Of-Flight Committee, LOI144, 2012. CERN-INTC-2012-019/INTC-I-144.
[45] J. Schell, D.C. Lupascu, J.G.M. Correia, A.W. Carbonari, M. Deicher, M.B. Barbosa, R.D. Mansano, K. Johnston, I.S. Ribeiro Jr., ISOLDE Collaboration, Hyper. Interact. 238 (2017) 2.
[46] D.V. Zyabkin, J. Schell, D. Gaertner, T.T. Dang, J.N. Gonçalves, G. Marschick, P. Schaaf, J. Appl. Phys. 126 (2019), 015102.
[47] K. Napo, F. Kadi Allah, J.C. Bernède, N. Barreau, A. Khelil, Thin Solid Films 427 (2003) 386.
[48] S. Ray, J. Dutta, K. Barua, S.K. Deb, Thin Solid Films 199 (1991) 201.
[49] Z.M. Jarzebski, J.P. Marton, J. Electrochem. Soc. 123 (1976) 199C.
[50] S. Samson, C.G. Fonstad, J. Appl. Phys. 44 (1973) 4618.
[51] G.N. Advani, P. Kluge-Weiss, R.L. Longini, A.G. Jordan, Int. J. Electron. 48 (1980) 403–411.